

An Experimental Study on Unsteady Flow Behaviors in an Axial-Flow Turbine

Shunsuke KASUGA¹, Atsumasa YAMAMOTO², Toshio MIYACHI³ and Takeshi OKANIWA⁴

¹ Graduate School of Tokyo Denki University

Ishizaka, Hatoyama-machi, Hiki-gun, Saitama 350-0394, JAPAN

Phone: +81-49-296-2911, FAX: +81-49-296-6544, E-mail: shunsuke@nal.go.jp

² Japan Aerospace Exploration Agency

7-44-1 Higashi-machi, Jindaiji, Choufu-shi, Tokyo 182-8522, JAPAN

Phone: +81-422-40-3444, E-mail: yamamoto.atsumasa@jaxa.jp

³ Tokyo Denki University

Ishizaka, Hatoyama-machi, Hiki-gun, Saitama 350-0394, JAPAN

Phone: +81-49-296-2911, FAX: +81-49-296-6544, E-mail: miya@n.dendai.ac.jp

⁴ Honda R&D Co., Ltd

3-15-1, Senzui, Asaka-shi, Saitama 351-0024, JAPAN

Phone: +81-48-464-2511, E-mail: Takeshi.Okaniwa@mail.a.rd.honda.co.jp

ABSTRACT

Using a high-response pressure sensor and a single-slanted hot-wire sensor, the upstream and the downstream flows of an annular turbine rotor were surveyed in detail. The data were time-split to produce animated movies, and the unsteady rotor-stator interaction and the associated secondary flow behaviors in the rotor passage were analyzed.

The loss decreases when the free stream part of the stator cascade is going to enter the downstream cascade passage and thus the flow will pass the rotor cascade smoothly. On the other hand, the loss increases when the stator wake will dominate the downstream rotor cascade passage.

NOMENCLATURE

C_{Pt}	= Total pressure loss coefficient, Eqs.(2),(3)
P_t	= Total pressure
P, Y, Z	= Coordinate laughs of pitch, yaw, axial directions
T	= Periodical time of rotor passing a stator
V_m	= Measured flow velocity (resultant velocity)
\overline{V}_S	= Secondary flow vector
V_p	= Spanwise flow velocity
V_Y	= Circumferential flow velocity
V_Z	= Axial flow velocity
W	= Projected velocity of V_m onto cylindrical surface
θ_P, θ_Y	= Pitch angle and yaw angle of flow
Ω	= Vorticity, Eq.(3)

(suffix)

P, Y, Z	= Pitch (spanwise direction), Yaw (circumferential) direction, Axial direction
S, R	= Stator, Rotor
a, r	= absolute, relative
in, out	= inlet, outlet
t	= time
$1, 2, 3$	= Plane1, Plane2, Plane3
$-$	= Pitch averaged
$=$	= Mass averaged (or cross sectional)
\equiv	= Overall mass averaged (or cross sectional and time averaged)

INTRODUCTION

To improve turbine efficiency further, it is necessary to understand the aerodynamic loss generation mechanisms in real turbines associated with the unsteady secondary flows such as passage vortices, blade tip leakage flow, endwall flows and so on. The mechanisms in real turbines are very complicated and difficult to understand because of the unsteadiness of such flows due to the interaction between stationary blades (stator) and moving blades (rotor). Such unsteady flows have often been studied and analyzed numerically recently but have not been studied experimentally so much due to many technical difficulties in such flow measurements. Most of the internal flow mechanisms, therefore, have only been guessed based on this limited data and the unsteady three-dimensional flows are difficult to understand because of extremely complex behaviors of the flows.

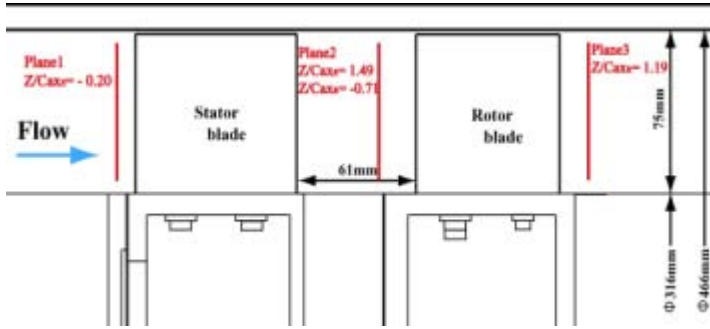


Fig.1 Low-speed turbine test rig

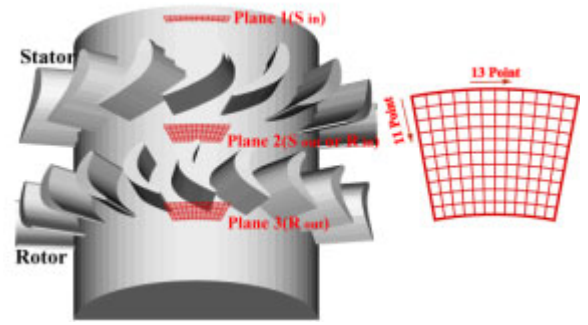


Fig.2 Measurement planes

This paper describes experimental results obtained with a high-response pressure sensor for unsteady total pressure measurement and a single-slanted hot-wire sensor for measure unsteady velocity and flow angle measurements. These measurements were made at three measuring planes before and behind the stator and the rotor. The data obtained were used to produce animated movies in order to see the unsteady flow behaviors easily. Time-averaged values are also presented to show unsteady performance of the test turbine.

EXPERIMENTAL METHOD

The test rig (Fig. 1) is a NAL's single stage low-speed axial-flow turbine test rig and is of an atmospheric suction type [1]. Straight blades having constant cross-section profiles along the blade spans are installed in the rig to make the stator and rotor cascades. The profiles are the same used in linear cascade tests [4,5]. Table 1 gives the specifications of the both cascades. These cascades were designed with relatively high loadings normally used in high-pressure stage turbines. The stator cascade itself can be rotated by a stepping motor for ease of the circumferential traverse measurement of the flow.

The rotor flow is the main objective to be analyzed in the present study. In this study, one measurement plane was located downstream of the stator (or upstream of the rotor), and one measurement plane was located downstream of the rotor as shown in Figs.1 and 2. The axial space between the stator trailing edge and downstream rotor leading edge is 61mm. A high-response pressure sensor and a single slanted hot-wire sensor were used to measure the unsteady flows with a synchronized measurement technique. From these date, serial instantaneous pictures of the flow with a certain time interval (i.e., at serial relative locations between the stator and the rotor) are obtained to make an animated movie. The measurement system is shown in Fig.3.

Table1 Major specifications of cascades

		Stator	Rotor
Blade number	N	16	20
Blade chord	C	104.4mm	73.5mm
Blade axial chord	C_{ax}	81.5mm	72.6mm
Blade span	H	75.0mm	75.0mm
Blade pitch	S	76.66mm	61.42mm
Blade camber angle	α_{in}	0.0deg	-49.8deg
Blade outlet camber angle	α_{out}	-68.0deg	63.5deg
Blade turning angle	$\Delta \alpha$	68.0deg	113.0deg
Design inlet flow angle	$\theta_{Y_{in}}$	0.0deg	-43.6deg
Design outlet flow angle	$\theta_{Y_{out}}$	-68.0deg	63.5deg
Design flow turning angle	$\Delta \theta$	68.0deg	107.1deg
Cascade stagger	ξ	-39.0deg	-17.0deg
Cascade aspect ratio	H/C	0.718	1.02
Cascade solidity	C/S	1.36	1.2
Leading-edge thickness ratio	$D(LE)/C$	0.127	0.111
Trailing-edge thickness ratio	$D(TE)/C$	0.033	0.056
Blade max thickness ratio	H_{max}/C	0.211	0.258
Hub / Tip diameter	D_{tip} / D_{hub}	316 / 466 mm	316 / 466 mm
Blade tip clearance	TCL	1.0mm	1.5mm

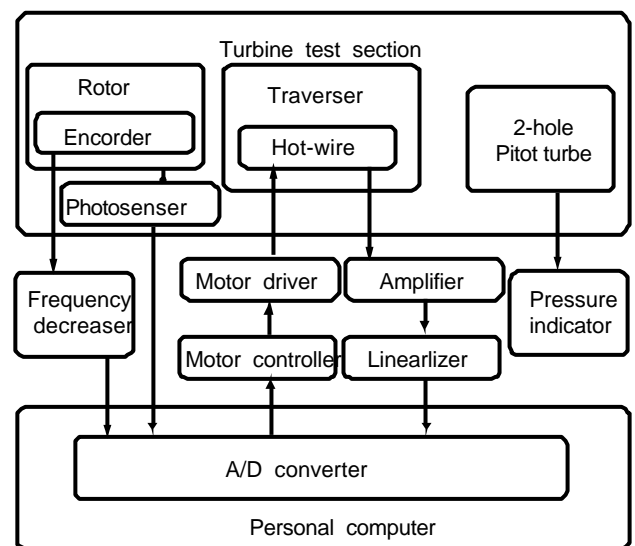


Fig.3 Unsteady flow measurement system

ANALYSIS METHOD

The method described by Kuroumaru et al.[2] was adopted to measure three-dimensional unsteady flows with somewhat different formula of calibration curve : a slanted single hot-wire probe was rotated several times, here twelve times, around its probe axis. We have adopted twelve times for the rotation and used the following formula to make the hot-wire calibration curves:

$$E = K(V)\{A(\gamma) + B(\gamma)\cos(\chi) + C(\gamma)\sin(\chi)\} \quad (1)$$

Here, E is the wire output voltage, $K(V)$ is expressed by a second order polynomial curve fitting of the flow velocity V , and $A(\gamma)$, $B(\gamma)$ and $C(\gamma)$ are expressed by third order polynomial ones of the pitch angle γ . χ is a geometrically determined angle from pitch angle γ , yaw angle of flow and the wire slanted angle. Totally fifteen coefficients included in K , A , B and C were determined from a calibration test which was conducted in the same atmospheric air condition just before the measurement starts.

For analyzing the secondary flow vector, the method described by Yamamoto et al.[3,4] was used. The secondary flow vector is defined as the vector component of the resultant velocity projected onto a plane normal to the mass-average mean flow direction. The mass-averaging was done in one stator cascade pitch for the stator flow analysis and one rotor cascade pitch for the rotor flow analysis.

Total pressure loss coefficient (CPT) was defined by the pressure drop from a cascade inlet to the same cascade outlet divided by the corresponding cascade outlet dynamic pressure. Therefore total pressure loss coefficients (CPT) can be written as follows;

$$CPT_S = \frac{Pt_{Sin} - Pt_{Sout}}{\frac{1}{2} \rho Vm_{Sout}^2} \quad \text{for stator} \quad (2)$$

$$CPT_R = \frac{Pt_{Rin} - Pt_R}{\frac{1}{2} \rho Vm_{Rout}^2} \quad \text{for rotor} \quad (3)$$

Vorticity was also calculated by the following equation and used to show local vortex distributions in the measurement planes in more detail than the secondary flow vectors show;

$$\Omega = \frac{\partial V_P}{\partial Y} - \frac{\partial V_Y}{\partial P} \quad (4)$$

EXPERIMENTAL RESULTS AND DISCUSSION

Overall view of the internal flows with animated 3D movies

Some animated movies were made in order to see the periodically unsteady flows of the stator and the rotor. Figure 4 shows a three-dimensional view of the inlet and the outlet

absolute velocities of the rotor at an instantaneous time. Here the absolute means values expressed in the absolute (stationary) frame of reference.

Figure 5(a) shows an unsteady absolute total pressure loss CPT_{Sa} of the stator at a certain time. Weak fluctuation of the loss can be recognized and is due to the effect of the rotor located downstream. Figure 5 (b) shows unsteady absolute total pressure loss CPT_{Ra} downstream of the rotor at the same instantaneous time.

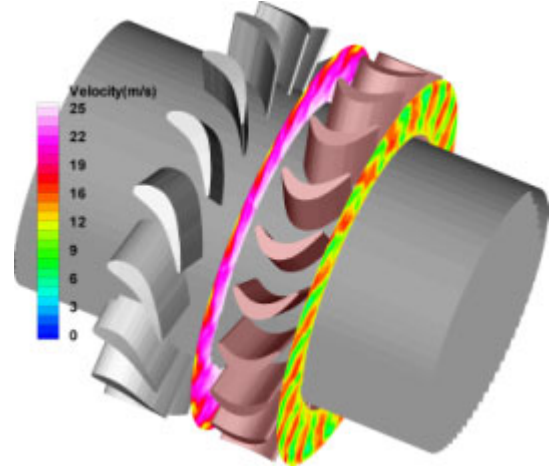
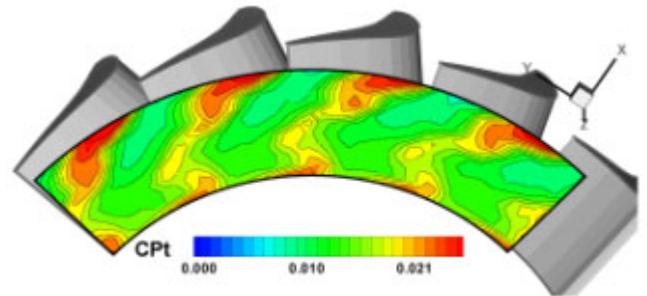
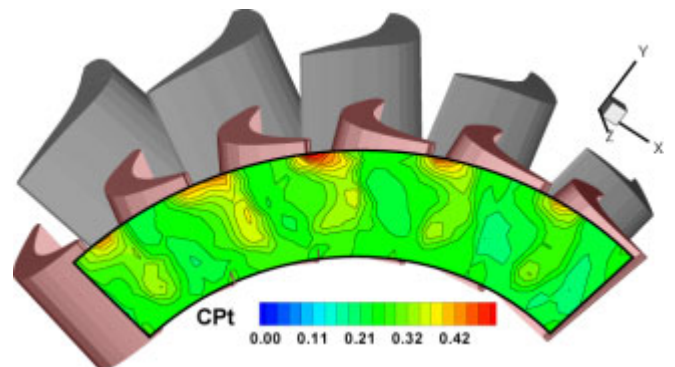


Fig.4 An overall view of the turbine unsteady internal flows (one frame of animated movie showing absolute inlet and outlet velocities at a certain instantaneous time)



(a) Unsteady absolute total pressure loss CPT_{Sa} downstream of the stator



(b) Unsteady absolute total pressure loss CPT_{Ra} downstream of the rotor

Fig.5 Animated movies of total pressure losses CPT_a

Detailed downstream flow field of the stator

Figure 6 shows time-averaged distributions of (a) absolute velocity V_{Sa} , (b) absolute secondary flow vectors V_{sSa} and absolute vorticity Ω_{Sa} and (c) absolute total pressure loss C_{PtSa} downstream of the stator. A region with locally minimum velocity is seen very close to the outer casing as shown by yellow color in Fig.6 (a) while in Fig.6 (b), locally minimum vorticity is seen a little apart from the casing (with negative value) as shown by blue color. The negative value of the vortex in this region means that the vortex is rotating clockwise and is considered to be generated by the leakage flow which passes the stator tip gap. Rotational direction of the secondary flow vectors there dose not coincide with the vorticity very well due to the different definitions of both flow and the secondary vorticity. In the present test case, note that some tip gap was left in the stator to ease the circumferential traverse measurements as described before although such tip gap does not normally exist in stators of real turbines. In the present annular

cascade, a pair of passage vortices could not be recognized so clearly not as was seen in linear cascades shown in [5]. This is due mainly to strong radial pressure gradient generated by swirling flows downstream of the annular stator cascade where the static pressure is higher at the tip side and lower at the hub side and therefore, the low energy fluids in the cascade wakes tend to be pushed toward the hub and the hub-side passage vortex is significantly deformed. As was explained by Yamamoto and Yanagi [1] with the same test rig, strong shedding vortices are generated just downstream of the stator trailing-edge. The detailed mechanism of the trailing-edge shedding vortex as indicated by SH here in figure 6(b) is explained in [1].

Figure 6(c) indicates two cores of locally maximum total pressure loss in the wake region as shown in red and yellow. The tip-side loss generated near the tip endwall is caused by the stator tip-leakage vortex TV and the tip-side passage vortex PV, while the hub-side loss is caused by the hub-side passage vortex PV and the shedding vortex SH.

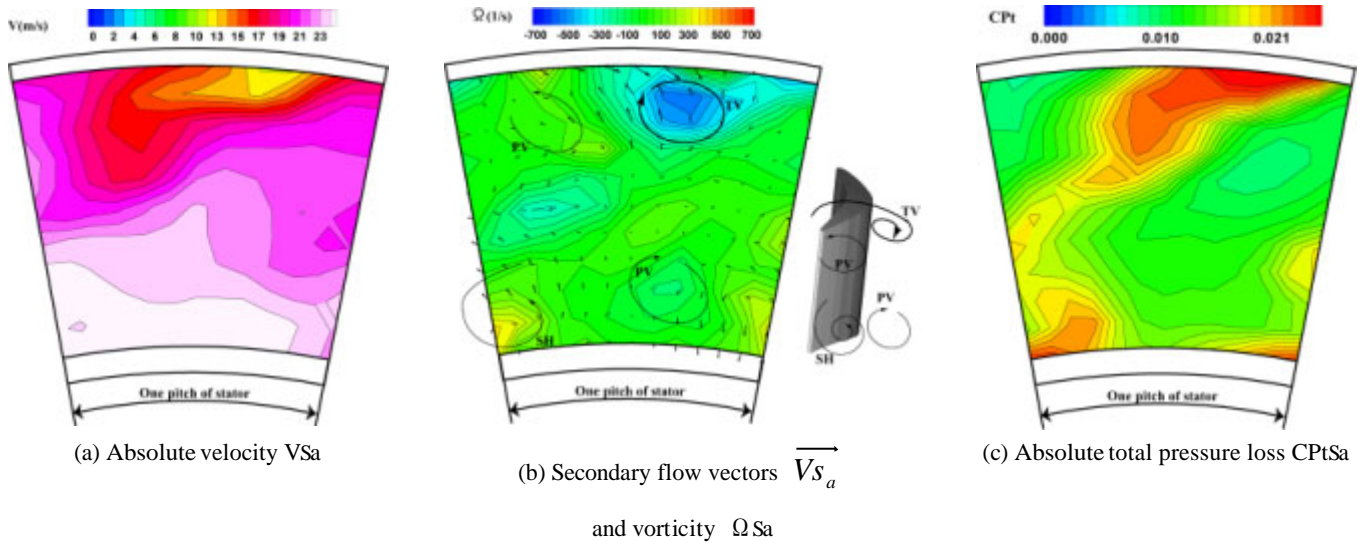


Fig.6 Time-averaged flow field downstream of the stator (absolute)

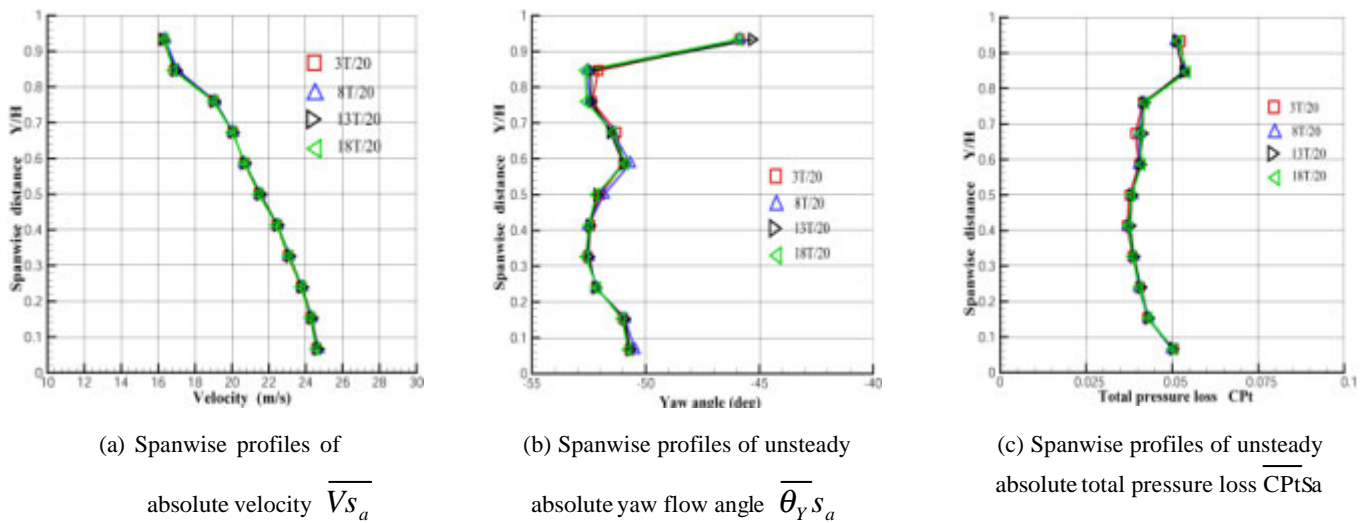


Fig.7 Spanwise profiles downstream of the stator (absolute)

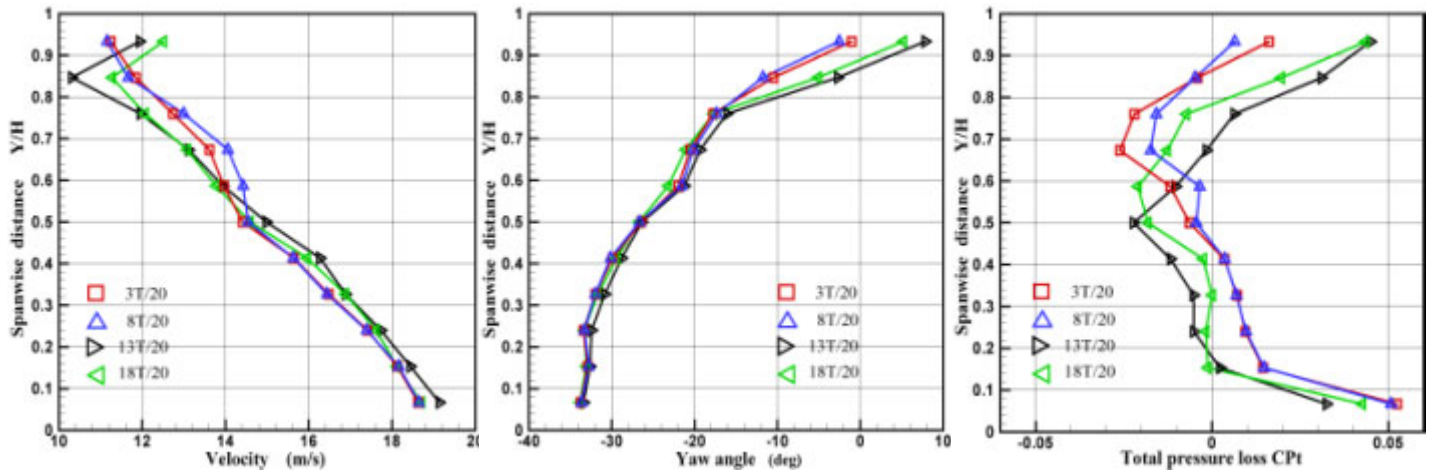
Figure 7 shows spanwise distributions of pitch-averaged values of instantaneous flows downstream of the stator; (a) absolute velocity, (b) absolute yaw flow angle and (c) absolute total pressure loss of the stator. In each figure, spanwise distribution lines at four instantaneous times are drawn. The time variations are very small in the absolute frame of reference, which shows very little effects of the rotor on the upstream flow field of the rotor.

When considering the rotor performance, the relative frame of reference will be adequate to use: Figure 8 indicates flow upstream rotor shown in the relative frame of reference. In this case, significant fluctuations appear in velocity, yaw flow angle and more significantly in the total pressure upstream of the rotor.

Detailed downstream flow field of the rotor

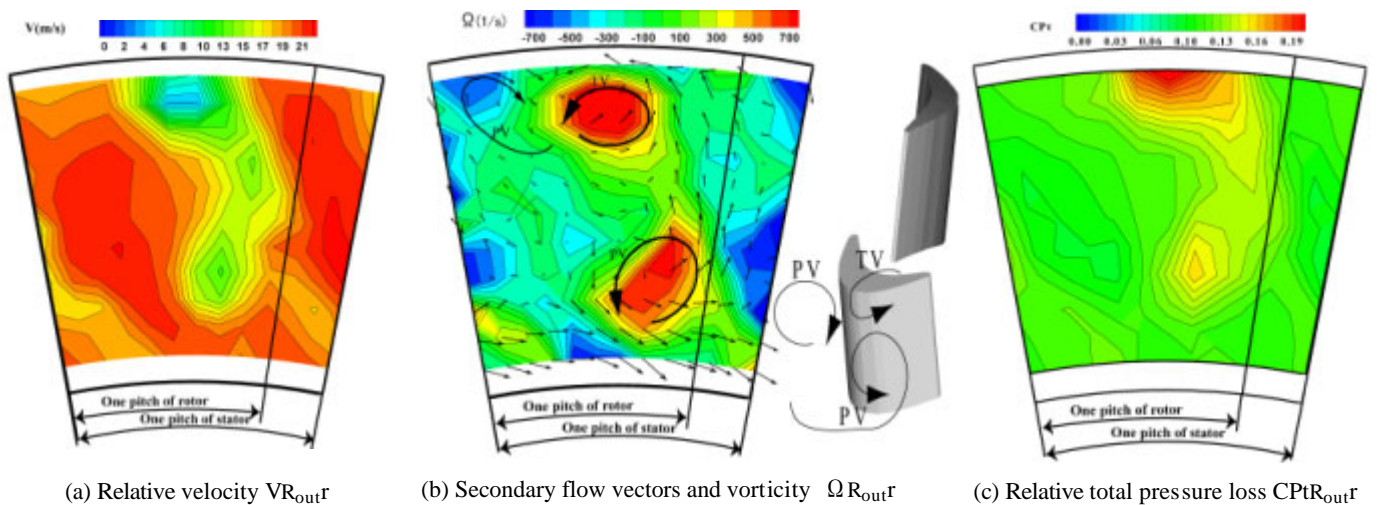
Figure 9(a)-(c) represents typical distributions at a certain instantaneous time of (a) velocity, (b) secondary flow and (c) total

pressure loss downstream of the rotor in the relative frame of reference to the rotor. The distributions shown here correspond to these in one stator cascade pitch, or 1.25 rotor cascade pitch. Lower velocity region (i.e., wake) is shown by green color in Fig.9 (a) where there are two locally minimum velocity cores. From vorticity distribution shown in Fig.9 (b) the tip-side core indicated in red color means that the vortex rotates counter-clockwise and is due to the leakage vortex (TV). On the other hand, the hub-side core corresponds to the hub-side passage vortex generated in the rotor. The tip-side passage vortex is difficult to see and can only be recognized at the left side of the tip-leakage vortex. Figure 9(c) shows total pressure loss distribution downstream of the rotor. The figure includes two cores of locally maximum total pressure losses in the wake region. The tip-side loss locates again very close to the tip casing where low energy fluids were accumulated mainly by the tip-leakage vortex and partly by the tip-side passage vortex (PV).



(a) Spanwise profiles of relative velocity $\overline{VR_{in r}}$ (b) Spanwise profiles of unsteady relative yaw flow angle $\overline{\theta R_{in r}}$ (c) Spanwise profiles of unsteady relative total pressure loss $\overline{CPr_{in r}}$

Fig.8 Spanwise profiles upstream of the rotor (relative)



(a) Relative velocity $\overline{VR_{out r}}$ (b) Secondary flow vectors and vorticity $\overline{\Omega R_{out r}}$ (c) Relative total pressure loss $\overline{CPr_{out r}}$

Fig.9 Unsteady flow distributions downstream of the rotor at t=13/20 (relative)

Figure 10(a) and (b) show fluctuations of pitch-averaged absolute yaw flow angle expressed in stationary frame of reference and relative yaw flow angle in rotational frame of reference, respectively. In this case, the pitch averaging was done in one rotor cascade pitch. Four lines in each figure show unsteady fluctuation of pitch-averaged yaw flow angle at four instantaneous times during one rotor-passing period T . In particular, the fluctuation is much larger in the tip-side half region compared to the hub-side half. The maximum fluctuation is reaches about 20 deg in absolute yaw flow angle and about 30 deg in relative yaw flow angle. Variations of the pitch-averaged values are important to note for designing the next blade rows downstream.

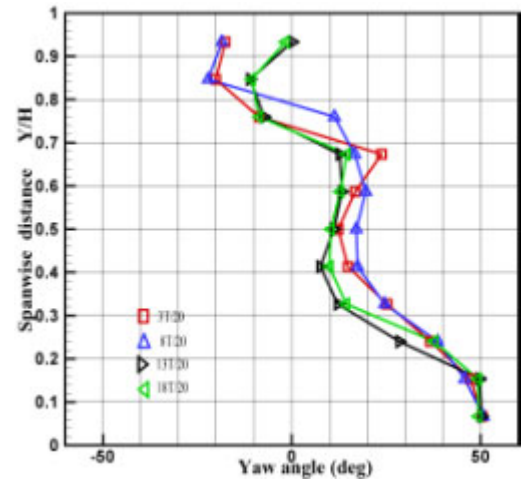
Figure 11 shows spanwise distributions of the rotor total pressure loss at four instantaneous times during a rotor-passing period T . The fluctuation is larger near the tip and smaller near the hub but is seen at almost whole span. The maximum fluctuation in the loss coefficient was about 0.07 (i.e., 48.2% of the overall mass-averaged value), which was occurred near the tip casing.

The unsteady loss distributions of the rotor at four selected times are schematically shown in figure 12. The loss variation is easily known in relation to the both cascade positions. Mass-averaged values of these figures 11 and 12 are shown in the next figure 13.

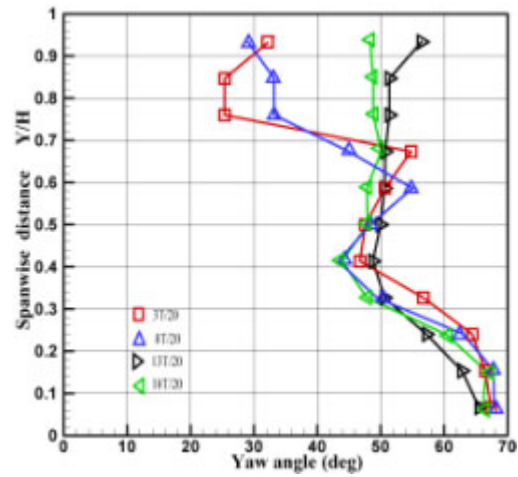
Figure 13 shows time variation of overall mass-averaged total pressure loss coefficient of the rotor during one rotor passing period T . The maximum variation of the mass-averaged loss is as large as 0.03 which corresponds to 24% of the time-averaged overall loss value. In the same figure, detailed total pressure distributions at the rotor inlet and the rotor outlet are also includes to show the conditions when the maximum and the minimum loss occur; Roughly speaking the maximum loss (0.144 at $3T/20$) seems to occur when an upstream stator wake is located at the suction side of the downstream rotor leading edges and at the pressure side of the downstream rotor hub leading-edge, respectively, while the minimum loss (0.114 at $13T/20$) occurs when an upstream wake is located at the leading edge of the downstream rotor. Considering the time gap until the wake in the upstream plane reaches the downstream plane, we guess that the loss decreases when the free stream part of the stator cascade is going to enter the downstream cascade passage and thus the flow will pass the rotor cascade smoothly. On the other hand, the loss increases when the stator wake will dominate the downstream rotor cascade passage. Further detailed discussion should be made on this clocking mechanisms by considering accurate time gap.

Figure 14 also shows effects of the stator-rotor interaction on velocity, vorticity / secondary flow vectors and total pressure loss fields in one periodical pitch (i.e., four stator cascade pitches or five rotor cascade pitches, or 90 deg) at a certain instantaneous time. All the values are shown in the relative (rotational) frame of reference: We can see, from different profiles of five rotor wakes,

not only instantaneous ‘spacial variations’ in one overall periodical pitch but also can know the ‘time variations’.



(a) Absolute yaw angle $\overline{\theta}_{Y_{Rout,a}}$



(b) Relative yaw angle $\overline{\theta}_{Y_{Rout,r}}$

Fig.10 Spanwise profiles of absolute and relative unsteady yaw flow angle

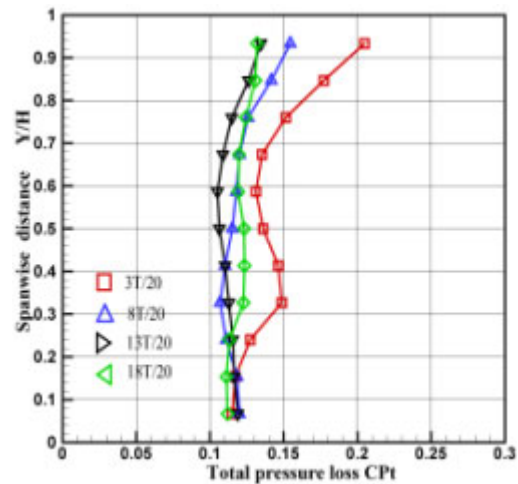


Fig.11 Spanwise distributions of unsteady total pressure loss ($\overline{Cp_t}_{R_{out,r}}$) of the rotor (relative)

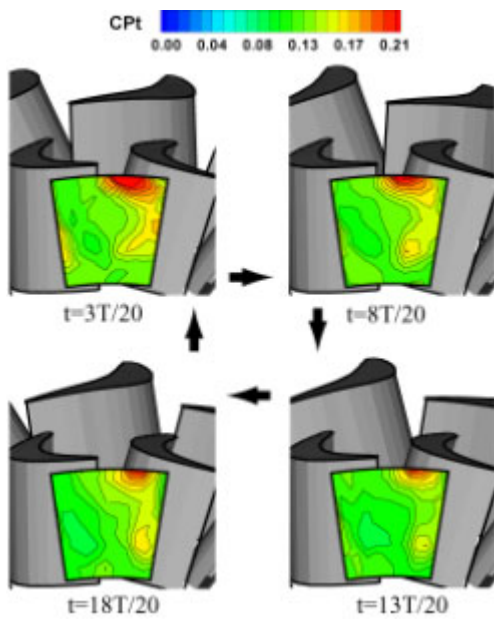


Fig.12 Unsteady relative total pressure loss ($Cp_{T_{RoutT}}$) downstream of the rotor (relative)

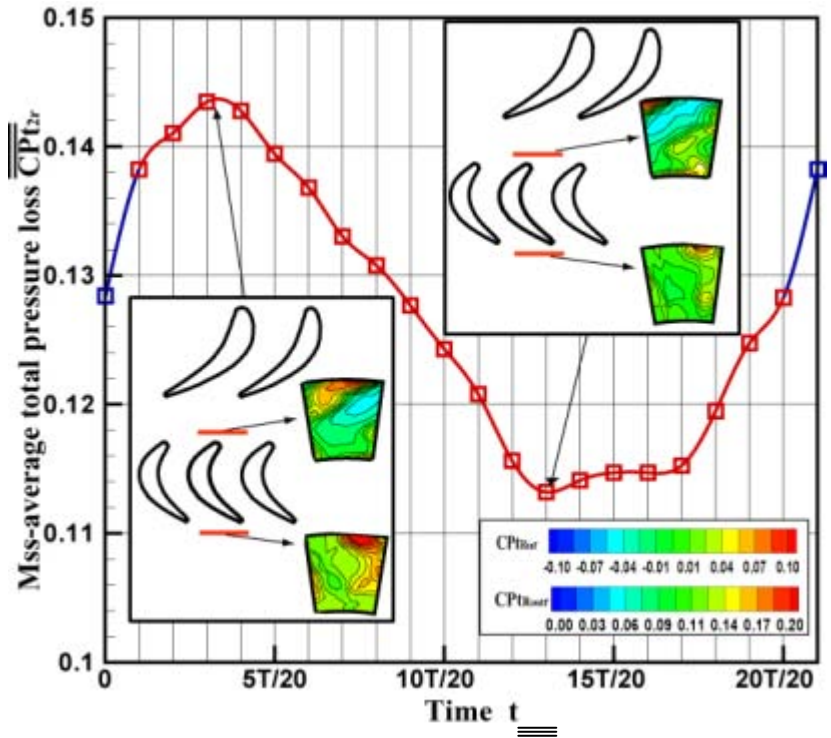


Fig.13 Unsteady overall total pressure loss ($Cp_{T_{RoutT}}$) of the rotor (relative, the stator and rotor profiles shown above correspond to those at the midspan)

CONCLUSIONS

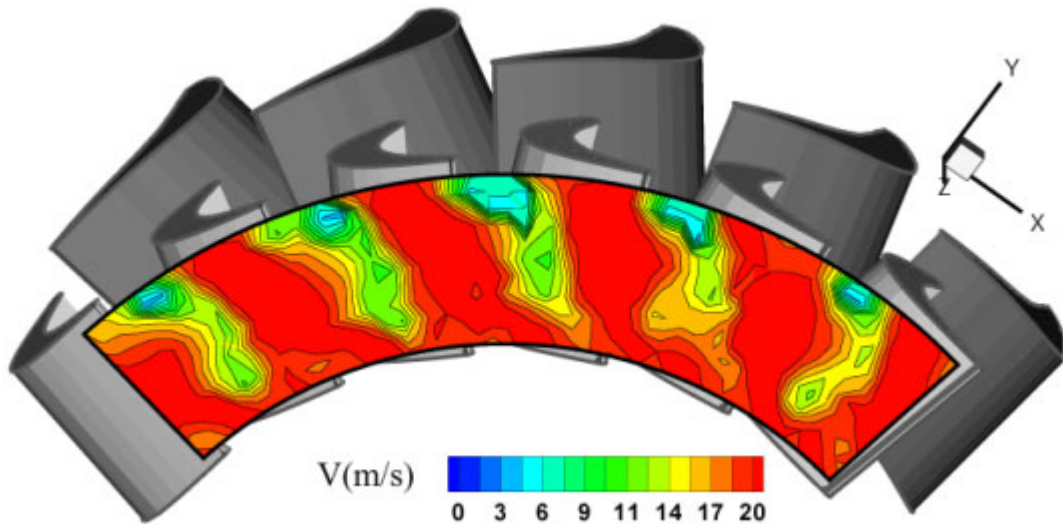
(1) Detailed measurements were made with a slanted hot wire and a high-respond total pressure probe to investigate three dimensional unsteady flows in an axial flow turbine, and unsteady flow behaviors caused by the stator-rotor interaction were made clear and visualized with animation movies produced from the measured data.

(2) Unsteadiness of flow quantities downstream of the rotor such as flow velocity, yaw flow angle and loss was presented and was generally much stronger at the tip-side half of the turbine flow passage. The unsteadiness is related to the vortex formation generated in the turbine stator and rotor passages. In the present test, the maximum variations was reaches as large as 20 and 30 deg in absolute and relative yaw flow angles respectively, and 24% of the time-averaged overall total pressure loss of the rotor.

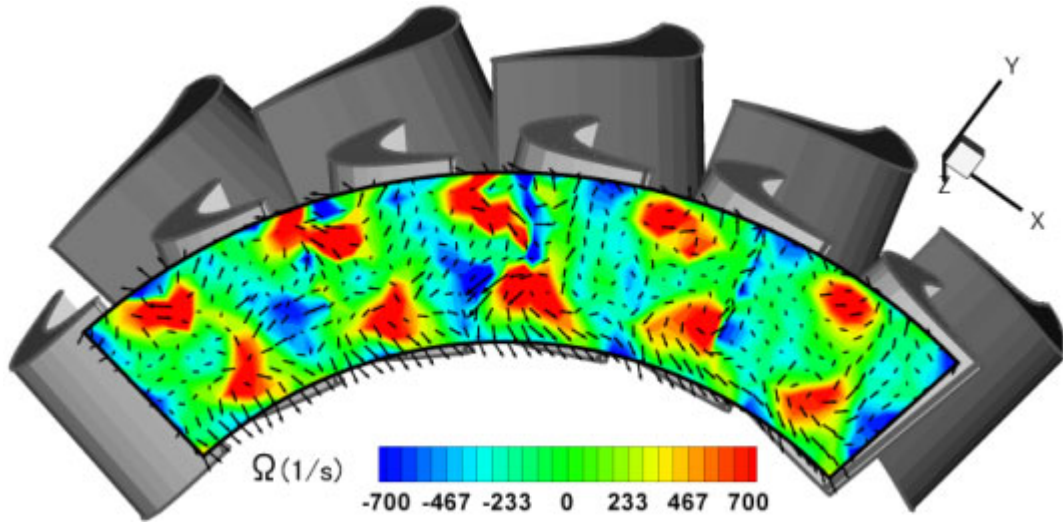
(3) The loss decreases when the free stream part of the stator cascade is going to enter the downstream cascade passage and thus the flow will pass the rotor cascade smoothly. On the other hand, the loss increases when the stator wake will dominate the downstream rotor cascade passage. Further detailed mechanisms on this effect, however, is open to discuss.

REFERENCES

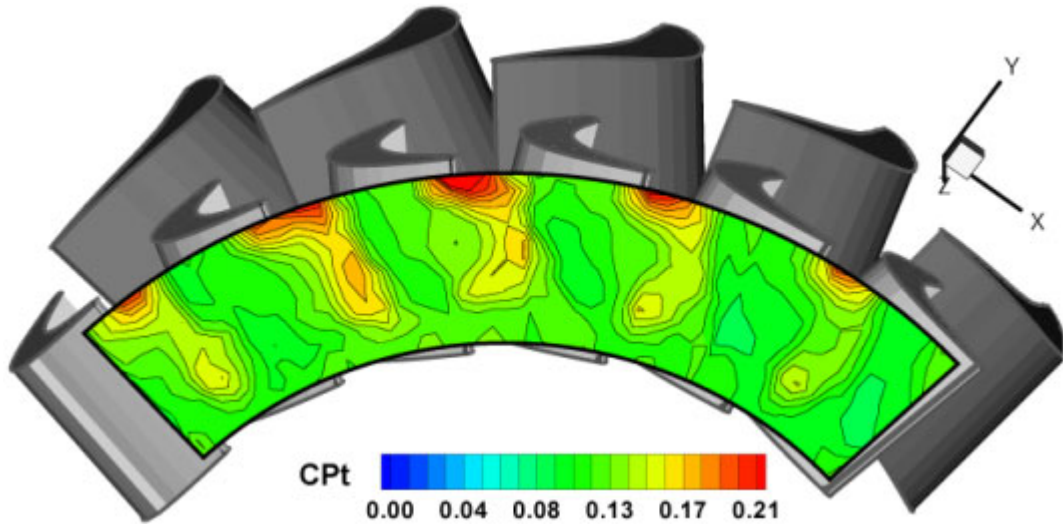
- [1] Yamamoto, A., and Yanagi, R., "Production and Development of Secondary Flows and Losses Within a Three Dimensional Turbine Stator Cascade" ASME Paper No.85-GT-217, 1985.
- [2] Kuroamaru, M., Inoue, M., Higaki, T., Abd-Elkhalek, F.A., and Ikui T., "Measurements of Three-Dimensional Flow Field Behind an Impeller by Means of Periodic Multi-Sampling of a Slanted Hot-Wire," Bulletin of JSME, Vol.25, No.209, 1982, pp.1674-1681.
- [3] Yamamoto, A., and Nouse, H., "Transient Phenomena of Secondary Flows and Losses Downstream of a Three Dimensional Turbine Stator Cascade With/Without the Effects of Hub Rotation and Hub Injection, " Symposium on Multi-Dimensional Fluid Transients, ASME Winter Annual Meeting, FED-Vol.18, 1984, pp.55-59.
- [4] Yamamoto, A., "Study of Internal Flow in Cooled Three Dimensional Blade Rows, Part1: Effects of Surface Injection on Secondary Flows and Pressure Losses in Stator," Trans. JSME (B), Vol.51, No.463, 1985, pp.829-838 (in Japanese).
- [5] Yamamoto, A., "Production and Development of Secondary Flows and Losses in Tow Types of Straight Turbine Cascades: Part1-A Stator Case", ASME Journal of Turbo machinery, Vol.109, 1987, pp.186-193.
- [6] Yamamoto, A., "Production and Development of Secondary Flows and Losses in Tow Types of Straight Turbine Cascades: Part2-A Rotor Case", ASME Journal of Turbo machinery, Vol.109, 1987, pp.194-200.



(a) Relative velocity $V_{R_{out}r}$



(b) Relative vorticity $\Omega_{R_{out}r}$



(c) Relative total pressure loss $CPt_{R_{out}r}$

Fig.14 Unsteady flows at plane3 downstream of the rotor (relative)